IAS Institut d'Astrophysique Spatiale Orsay

université PARIS-SACLAY

cea irfu

Cosmological constraints from the Chandra-Planck galaxy cluster sample

Gaspard Aymerich

Marian Douspis, Laura Salvati
Institut d'Astrophysique Spatiale

Gabriel Pratt
Astrophysique Interactions Multi-Echelles, CEA

Felipe Andrade-Santos, William Forman, Christine Jones
Center for Astrophysics, Harvard

Theoretical background

Cosmology:
Find a theoretical model capable of explaining the entire evolution of the Universe

Current model: ΛCDM model, expanding universe with cold dark matter

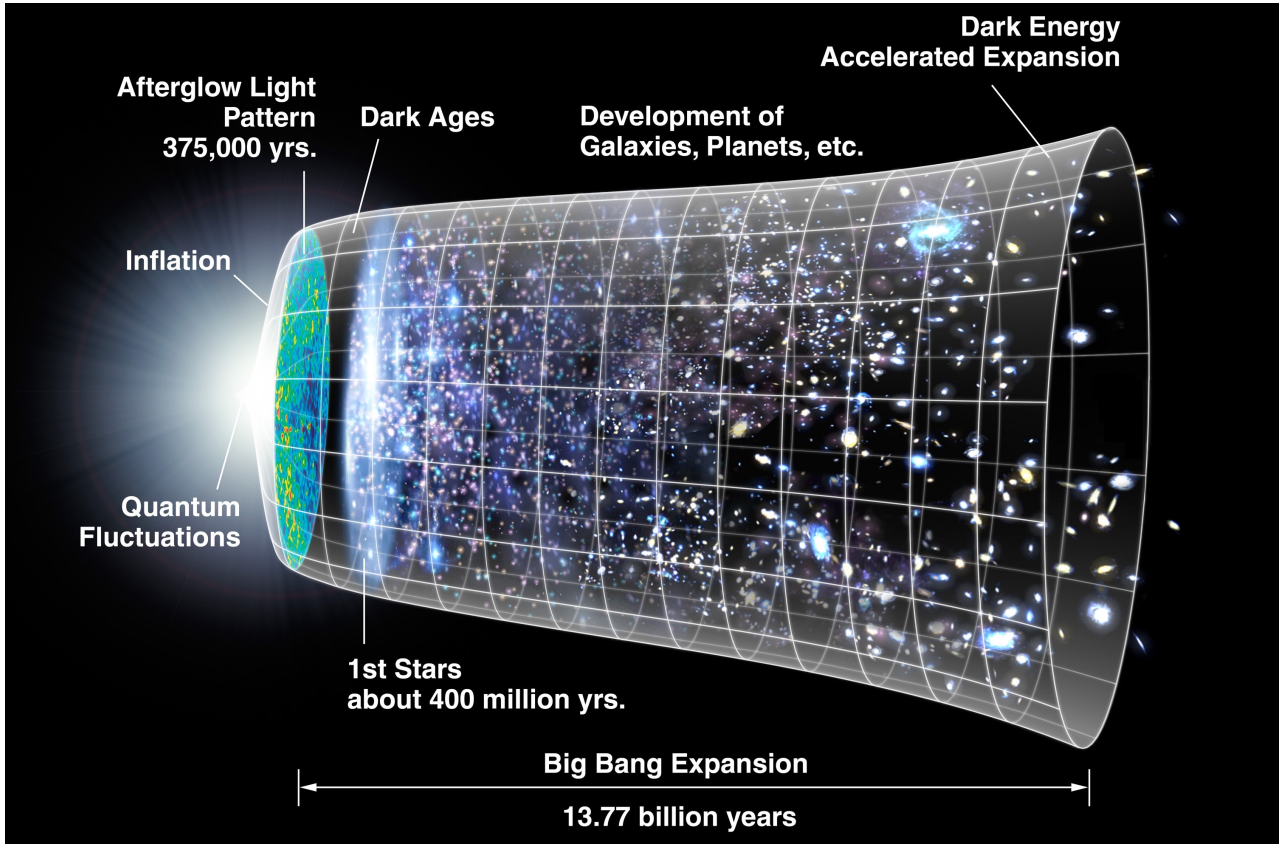

Hubble Space Telescope Science Institute

Examples of probes:
- Cosmic Microwave Background
- Galaxy clustering
- Galaxy lensing
- Supernovae
- Gravitational waves
- **Galaxy clusters**

Formation of structures

Halo formation:

Primordial Universe: overall homogeneous with small spatial density variations

Gravitationally unstable: over-densities attract more matter and grow over time

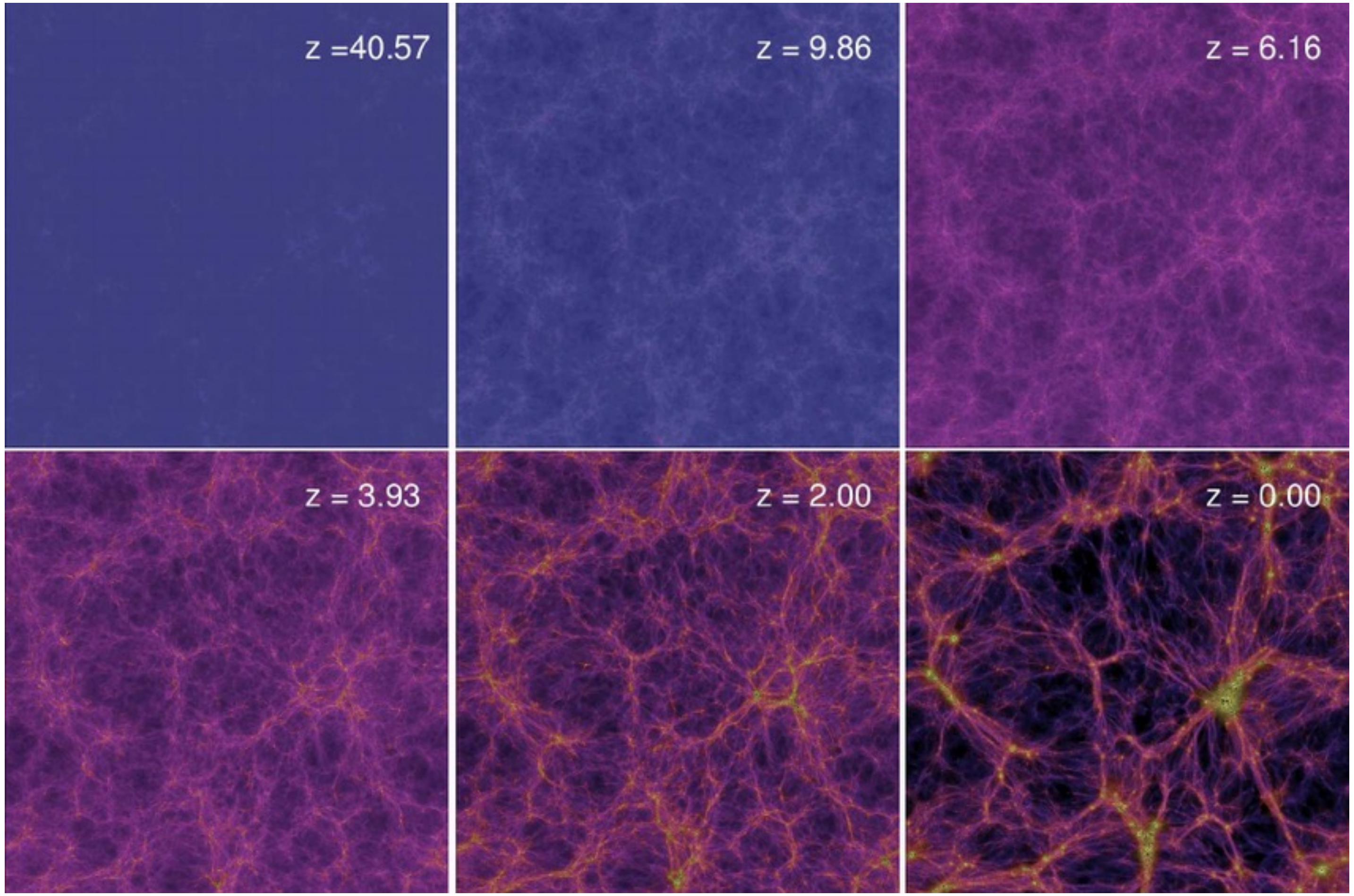

Zhao et al. 2012

Gravitational collapse & expansion of Universe: Formation of a cosmic web, with extreme overdensities at the nodes, **galaxy clusters**

« Typical » galaxy cluster:
1 Mpc, $5.10^{14} M_{\odot}$, a few billion light-years away

80% dark matter
16% hot gas (>1 keV)
4% stars

Galaxy clusters & cosmology

How can galaxy clusters be used as a cosmological probe ?

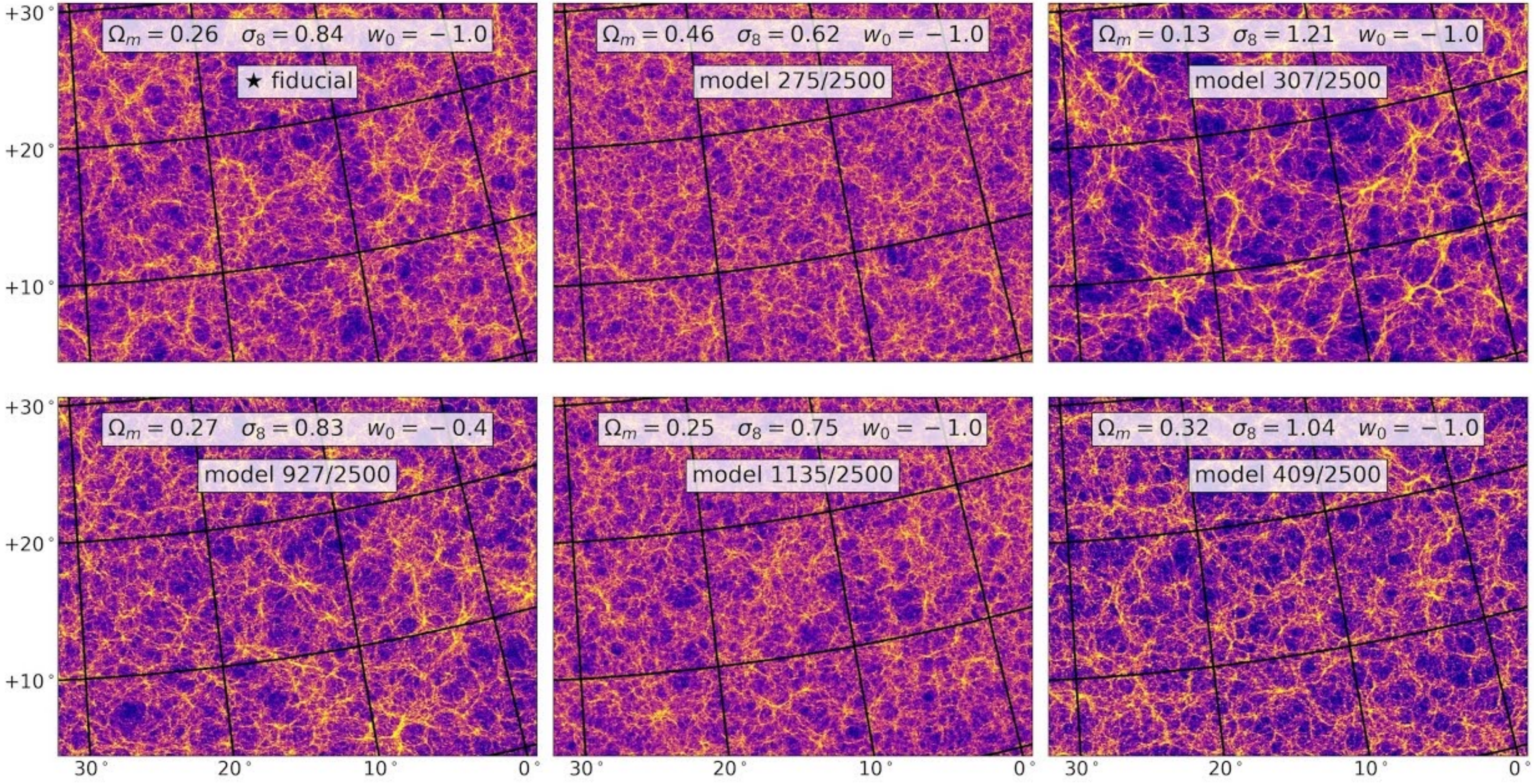

cosmogrid.ai

The formation of structures depends on the underlying cosmological model,
leading to **different populations of galaxy clusters**

How can galaxy clusters be used as a cosmological probe ?

Mass function: theoretical **prediction of cluster abundance** as function of **mass and redshift**

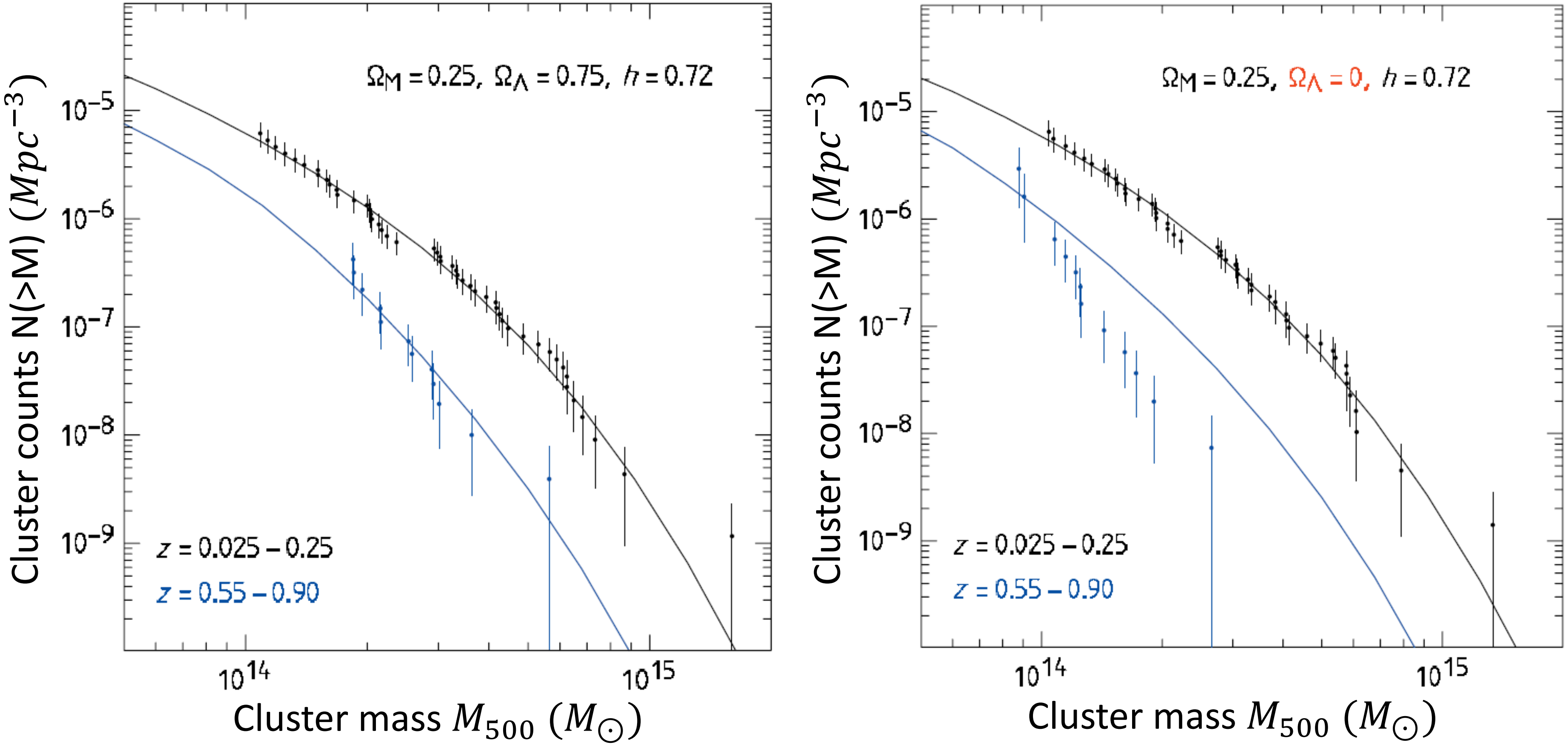

Vikhlinin et al. 2009

Observing galaxy clusters

How can we observe them ?

Different wavelengths probe different properties of clusters

Combining all wavelengths allow for more precise characterisation of cluster properties

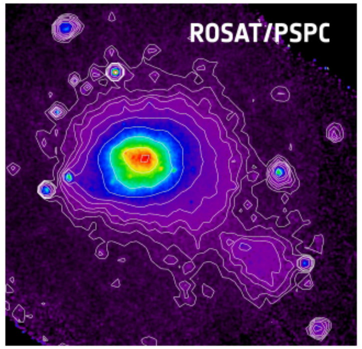

X-ray emission:
Bremmstrahlung
Sensitive to **gas density squared**
High resolution

$$E_X \propto \int_V n_e^2 \Lambda(T) dV$$

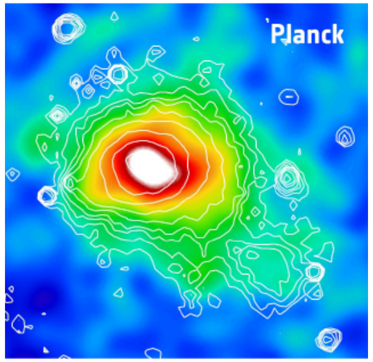

mm-wavelength:
Thermal Sunyaev-Zeldovich effect
(inverse Compton scattering)
Sensitive to **gas pressure**

$$F_\nu \propto \int_\Omega (P = n_e T) d\Omega$$

Optical/near IR wavelength:
Stars (small part of total mass)
Gravitational lensing
(total mass, limited precision)

Combining X-ray and SZ

Improving on Planck 2015: a better calibration sample

Planck data provides full sky SZ-survey: great opportunity for cosmological analysis

Cluster mass can't be directly inferred from SZ signal

X-ray observations allow for mass estimations under hydrostatic equilibrium assumption

Y500-M500 is calibrated on a common XMM/SZ set of 71 clusters: $E^{-2/3}(z)\left[\frac{D_A^2\, Y_{500}}{10^{-4}\,\mathrm{Mpc}^2}\right] = 10^{-0.19\pm0.02}\left(\frac{(1-b)\,M_{500}}{6\times10^{14}\,M_\odot}\right)^{1.79\pm0.08}$

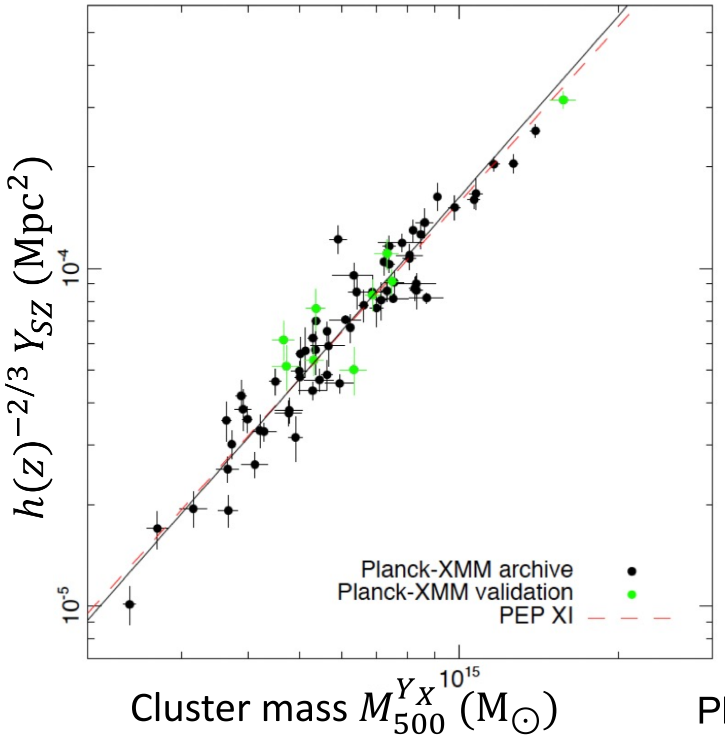

Planck 2013

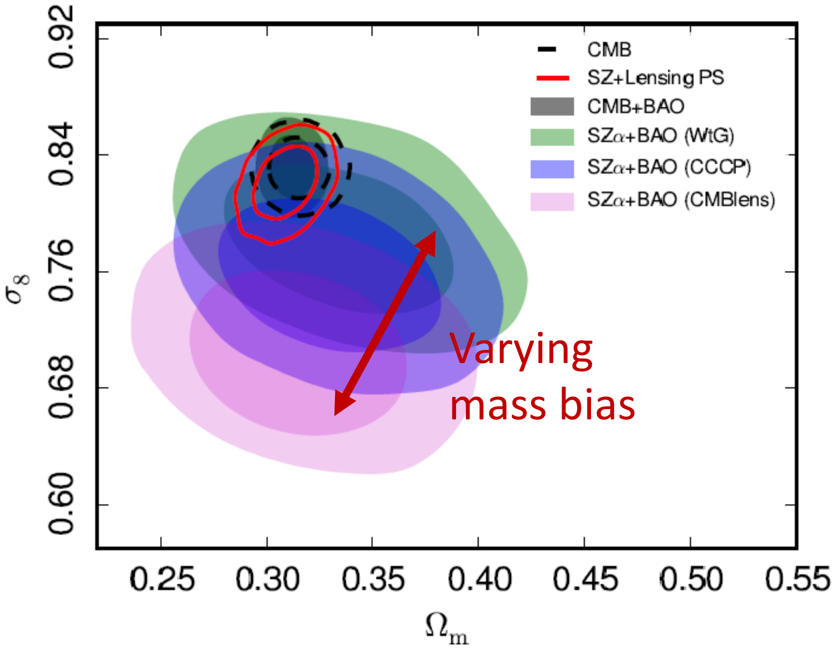

Planck 2015

Combining X-ray and SZ

Improving on Planck 2015: a better calibration sample

Planck data provides full sky SZ-survey: great opportunity for cosmological analysis

Cluster mass can't be directly inferred from SZ signal

X-ray observations allow for mass estimations under hydrostatic equilibrium assumption

Y500-M500 is calibrated on a common XMM/SZ set of 71 clusters: $E^{-2/3}(z)\left[\frac{D_A^2\,Y_{500}}{10^{-4}\,\mathrm{Mpc}^2}\right] = 10^{-0.19\pm0.02}\left(\frac{(1-b)\,M_{500}}{6\times10^{14}\,M_\odot}\right)^{1.79\pm0.08}$

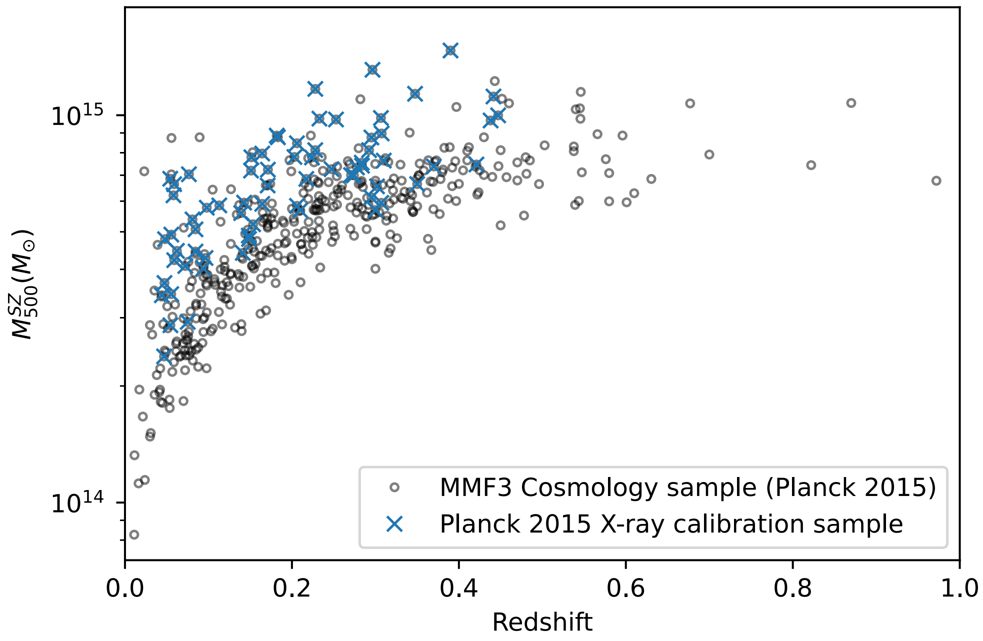

Combining X-ray and SZ

Improving on Planck 2015: a better calibration sample

Planck data provides full sky SZ-survey: great opportunity for cosmological analysis

Cluster mass can't be directly inferred from SZ signal

X-ray observations allow for mass estimations under hydrostatic equilibrium assumption

~~Y500-M500 is calibrated on a common XMM/SZ set of 71 clusters:~~ $E^{-2/3}(z)\left[\frac{D_A^2\, Y_{500}}{10^{-4}\,\mathrm{Mpc}^2}\right] = 10^{-0.19\pm0.02}\left(\frac{(1-b)\,M_{500}}{6\times10^{14}\,M_\odot}\right)^{1.79\pm0.08}$

Full re-observation of Planck ESZ sample (with z<0.35) by Chandra

SZ-selected sample
More clusters (146 vs 71)
Better low-mass leverage
Similar high-mass leverage
Better low-redshift leverage
Slightly worse high-redshift leverage

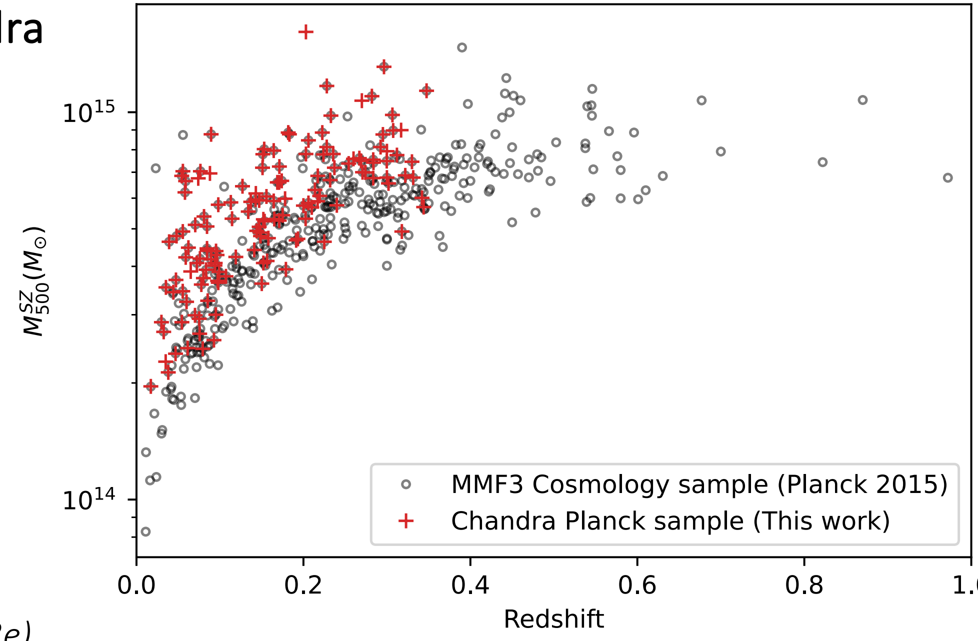

Work done by CfA team (Santos et al. 2021, https://doi.org/10.3847/1538-4357/abf73e)

Combining X-ray and SZ

Improving on Planck 2015: a better calibration sample

Planck data provides full sky SZ-survey: great opportunity for cosmological analysis

Cluster mass can't be directly inferred from SZ signal

X-ray observations allow for mass estimations under hydrostatic equilibrium assumption

~~Y500-M500 is calibrated on a common XMM/SZ set of 71 clusters:~~ $E^{-2/3}(z)\left[\frac{D_A^2\, Y_{500}}{10^{-4}\,\mathrm{Mpc}^2}\right] = 10^{-0.19\pm0.02}\left(\frac{(1-b)\,M_{500}}{6\times10^{14}\,M_\odot}\right)^{1.79\pm0.08}$

146 clusters from Planck ESZ sample were observed by Chandra

Analyse the data and calibrate a new scaling relation
Constrain cosmological parameters

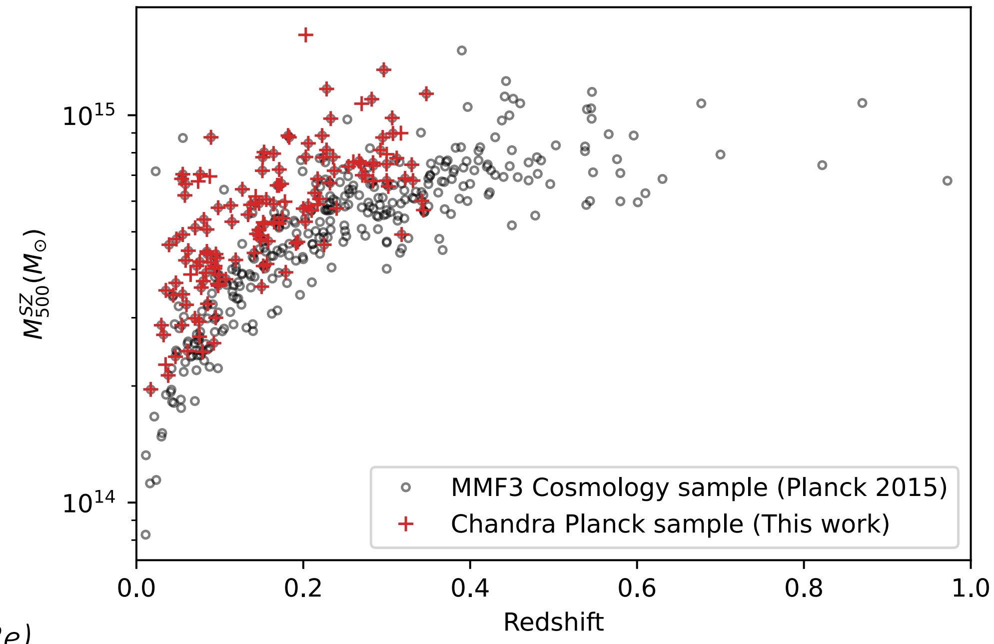

Work done by CfA team (Santos et al. 2021, https://doi.org/10.3847/1538-4357/abf73e)

Combining X-ray and SZ

Improving on Planck 2015: a better calibration sample

Planck data provides full sky SZ-survey: great opportunity for cosmological analysis

Cluster mass can't be directly inferred from SZ signal

X-ray observations allow for mass estimations under hydrostatic equilibrium assumption

~~Y500-M500 is calibrated on a common XMM/SZ set of 71 clusters:~~ $E^{-2/3}(z)\left[\frac{D_A^2\, Y_{500}}{10^{-4}\,\mathrm{Mpc}^2}\right] = 10^{-0.19\pm0.02}\left(\frac{(1-b)\,M_{500}}{6\times10^{14}\,M_\odot}\right)^{1.79\pm0.08}$

146 clusters from Planck ESZ sample were observed by Chandra

↓

Analyse the data and calibrate a new scaling relation
Constrain cosmological parameters

Analysis of the raw data up to X-ray derived masses done by collaborators at CfA

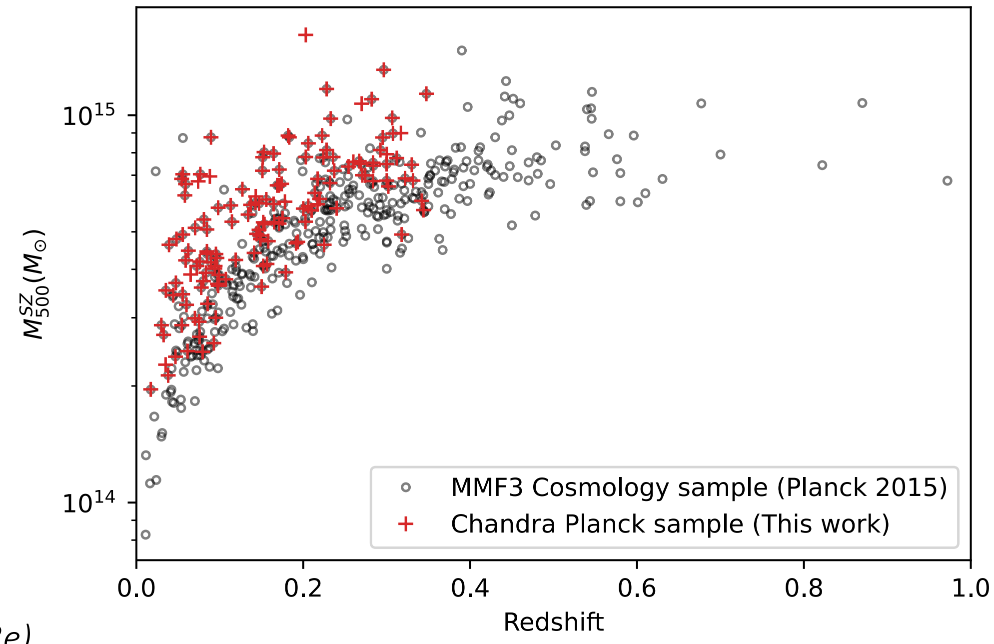

Work done by CfA team (Santos et al. 2021, https://doi.org/10.3847/1538-4357/abf73e)

Obtaining masses

Calibrating the Ysz-M relation

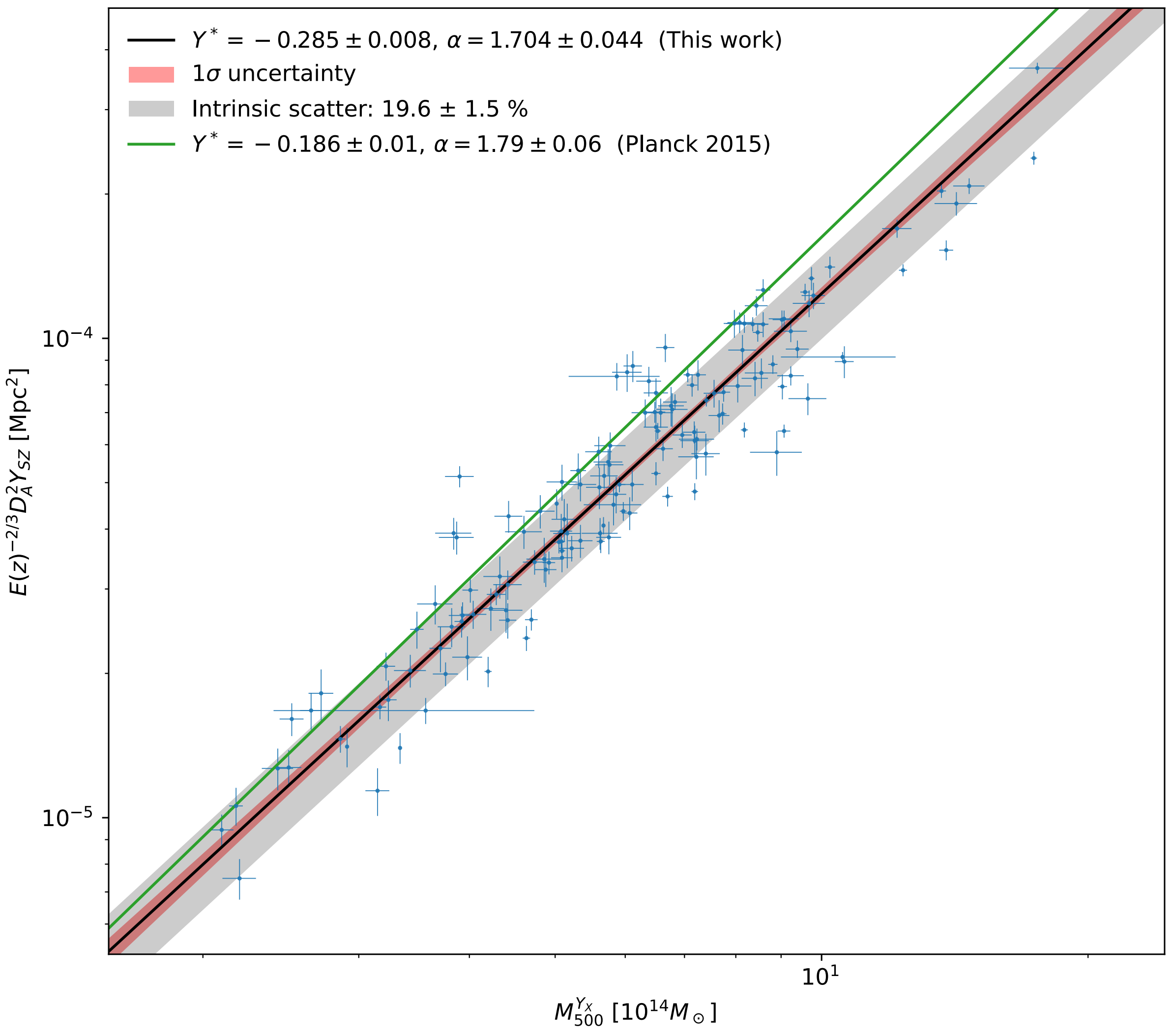

Run **MMF algorithm with X-ray positions and apertures**
Obtain Ysz with uncertainties

Correct for Malmquist bias:
Divide each individual Ysz by mean bias at that value

After **adding statistical uncertainty and scatter from X-ray scaling relation**:

$$E^{-2/3}(z)\frac{D_A^2\,Y_{500}}{10^{-4}\mathrm{Mpc}^2} = 10^{-0.29\pm0.01}\left(\frac{(1-b)M_{500}}{6\cdot10^{14}M_\odot}\right)^{1.70\pm0.1}$$

Scatter: 21%

Obtaining masses

Comparison with Planck 2015 results

Preliminary scaling relation:

$$E^{-2/3}(z)\frac{D_A^2\, Y_{500}}{10^{-4}\mathrm{Mpc}^2} = 10^{-0.29\pm0.01}\left(\frac{(1-b)M_{500}}{6\cdot 10^{14}M_\odot}\right)^{1.70\pm0.1}$$

Scatter: 21%

Planck collab. 2015 Cosmology from SZ number counts scaling relation :

$$E^{-2/3}(z)\left[\frac{D_A^2\, Y_{500}}{10^{-4}\,\mathrm{Mpc}^2}\right] = 10^{-0.19\pm0.02}\left(\frac{(1-b)\,M_{500}}{6\times 10^{14}\,M_\odot}\right)^{1.79\pm0.08}$$

Scatter: 18%

The new scaling relation has:
Lower normalization: Chandra and XMM temperature calibration don't match, Chandra measures hotter and thus heavier clusters. The **difference is coherent with predictions from Schellenberger et al. 2015** (20% difference)

Shallower slope: The new scaling relation is closer to self-similar (slope of 5/3)

Comparable uncertainties: Lower uncertainties on Y_{SZ}-M_{Y_X} (larger sample) but higher uncertainties on Y_X-M_{Y_X} compensates the difference

Obtaining masses

Calibrating the hydrostatic mass bias

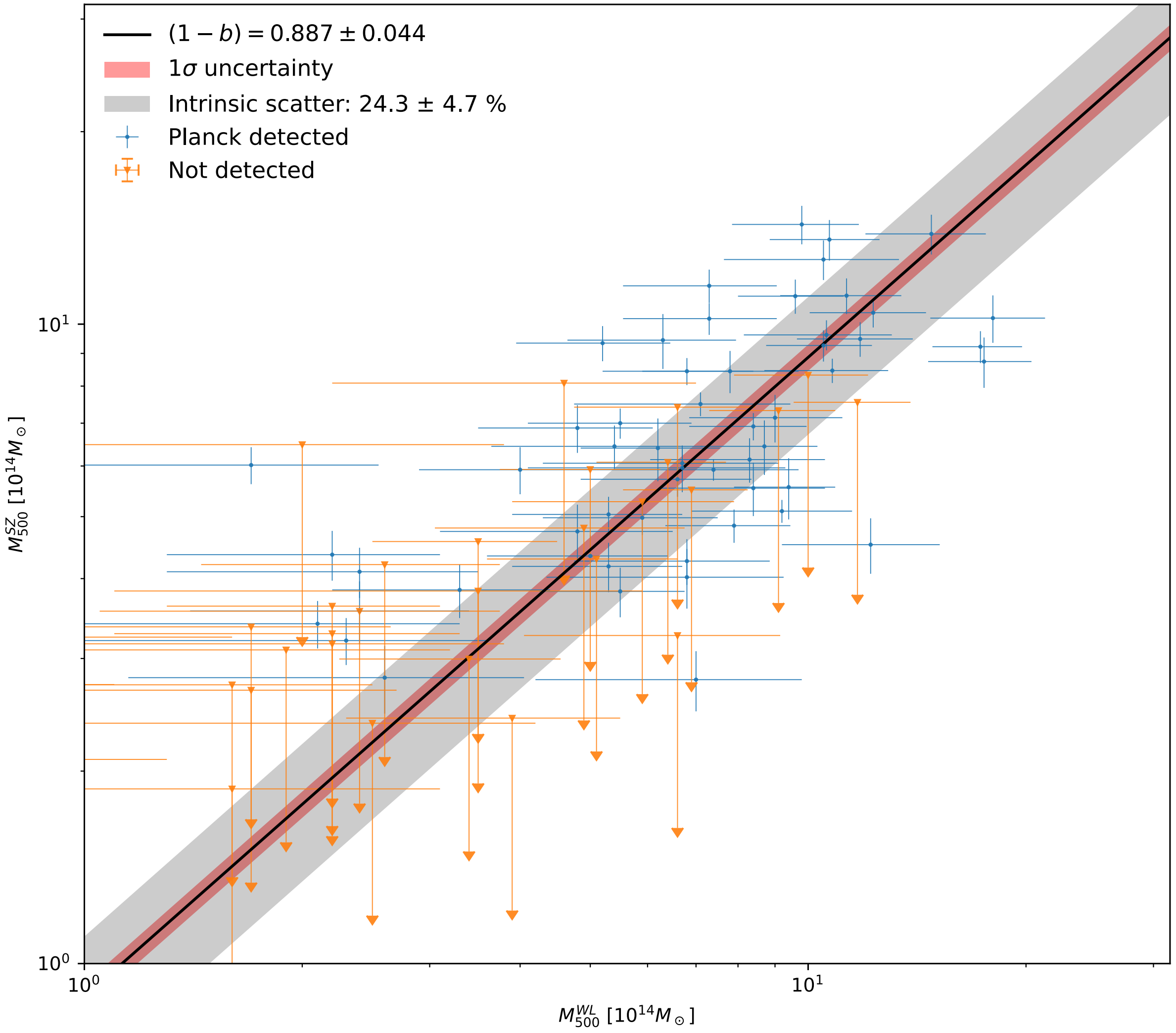

X-Ray masses are obtained under the assumption of hydrostatic equilibrium (i.e. thermal pressure perfectly balancing gravity)

Non thermal pressure support and deviations from equilibrium lead to **under-estimation of the true mass**

Effect accounted for by a **multiplicative factor, calibrated with weak lensing mass estimates**

$$E^{-2/3}(z)\,\frac{D_A^2\,Y_{500}}{10^{-4}\mathrm{Mpc}^2} = 10^{-0.29\pm0.01}\left(\frac{(1-b)M_{500}}{6\cdot10^{14}M_\odot}\right)^{1.70\pm0.1}$$

Use WL data from Herbonnet et al. 2020

Calibration sample	D+nD	D
Chandra	0.89 ± 0.04	0.91 ± 0.05
XMM-Newton	0.76 ± 0.04	0.78 ± 0.04
Herbonnet+20	X	0.81 ± 0.04
CCCP (P15)	X	0.78 ± 0.09

Constraining the cosmology

Final cosmological constraints

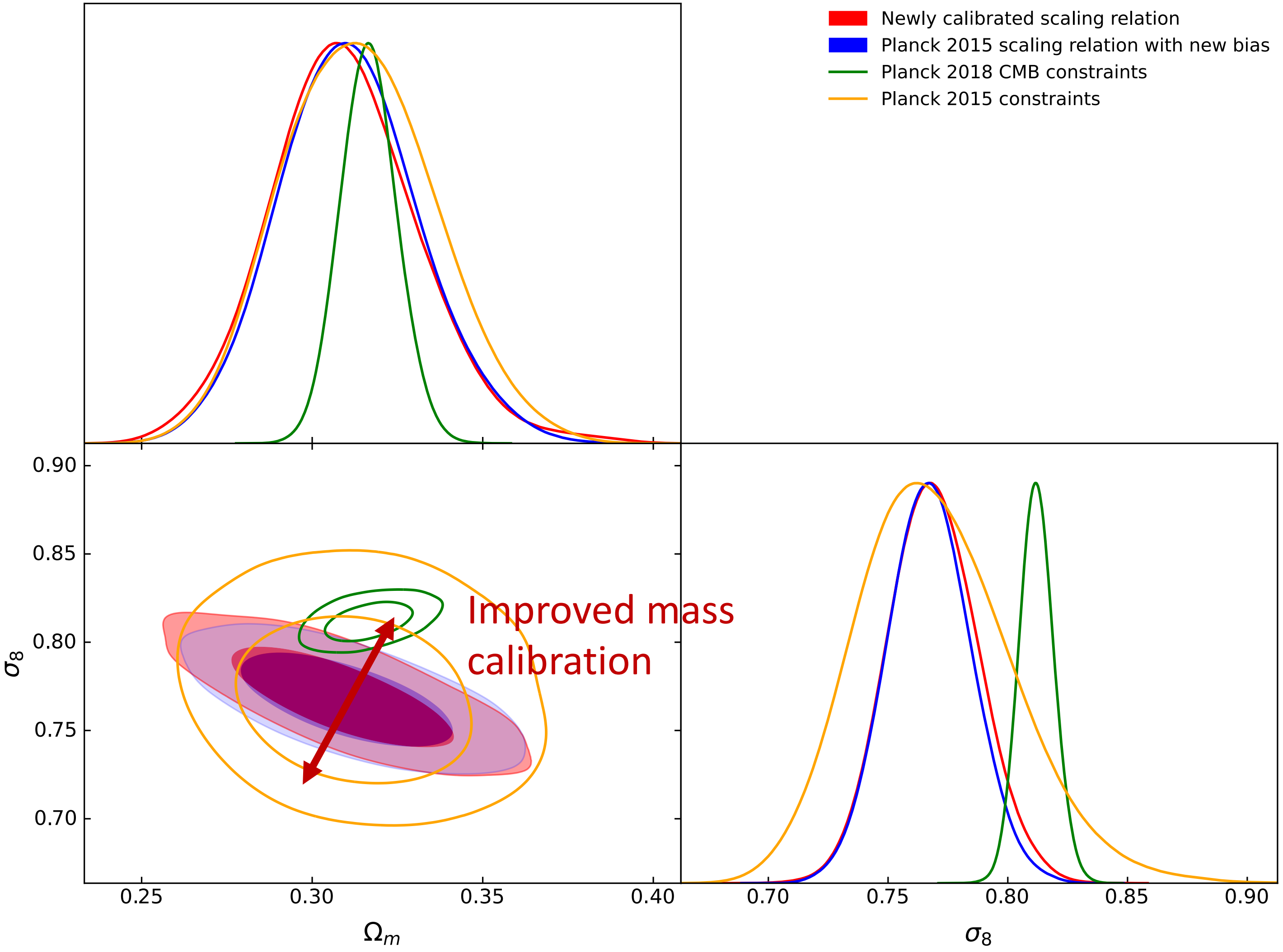

Cosmological constraints obtained:

X-ray sample	Ω_m	σ_8
Chandra	0.308 ± 0.022	0.764 ± 0.019
XMM-Newton	0.311 ± 0.020	0.755 ± 0.019

Even with **calibration problems** between the two telescopes, **the constraints are fully consistent**

Constraints are **centered on the same value and tighter than Planck 2015**, thus in **higher tension with the CMB**

Mass calibration, and **mass bias in particular is the most sensitive point of cluster cosmology**

Bonus: Redshift dependance

Redshift dependance was fixed to self-similar value: can we constrain it from the data ?

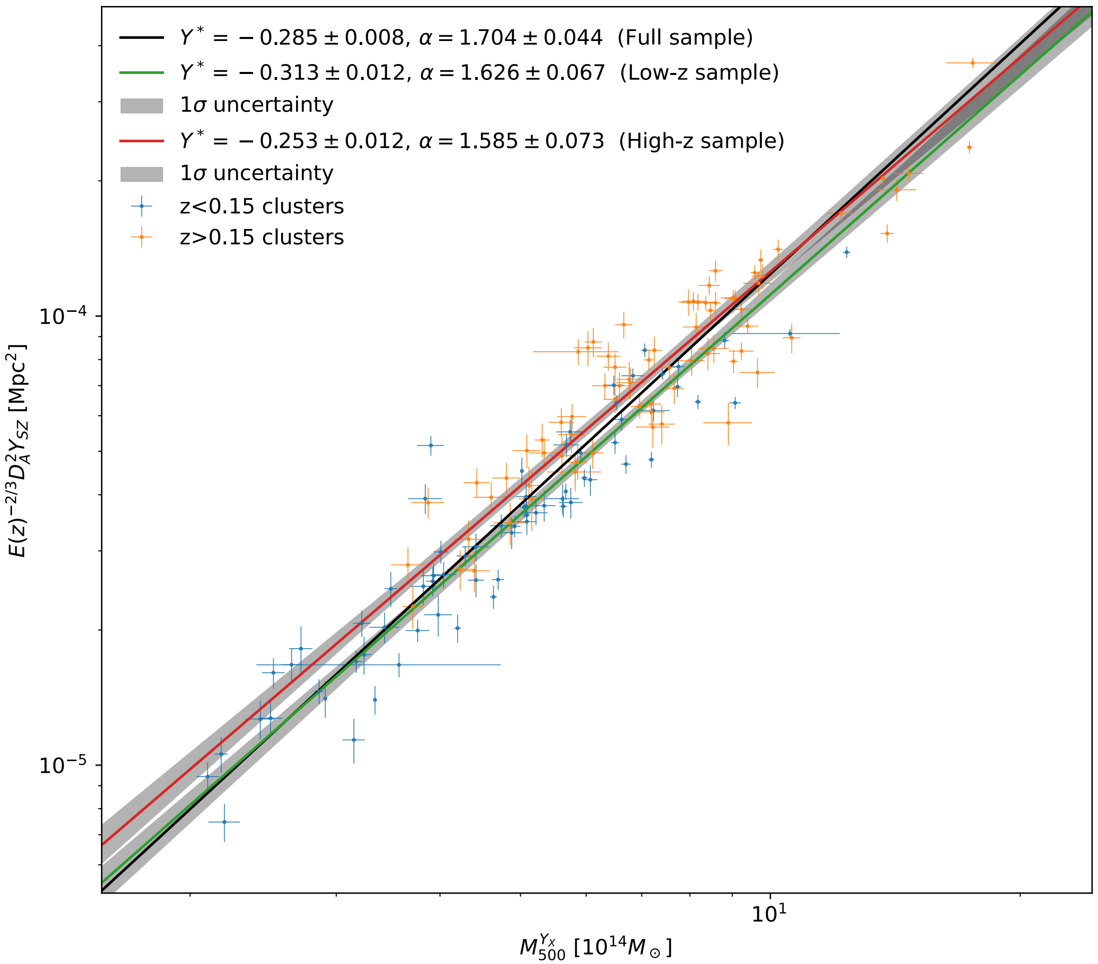

Motivation for investigation:

Separating the calibration sample into **high-z and low-z subsamples yields different best fits**

Bonus: Redshift dependance

Redshift dependance was fixed to self-similar value: can we constrain it from the data ?

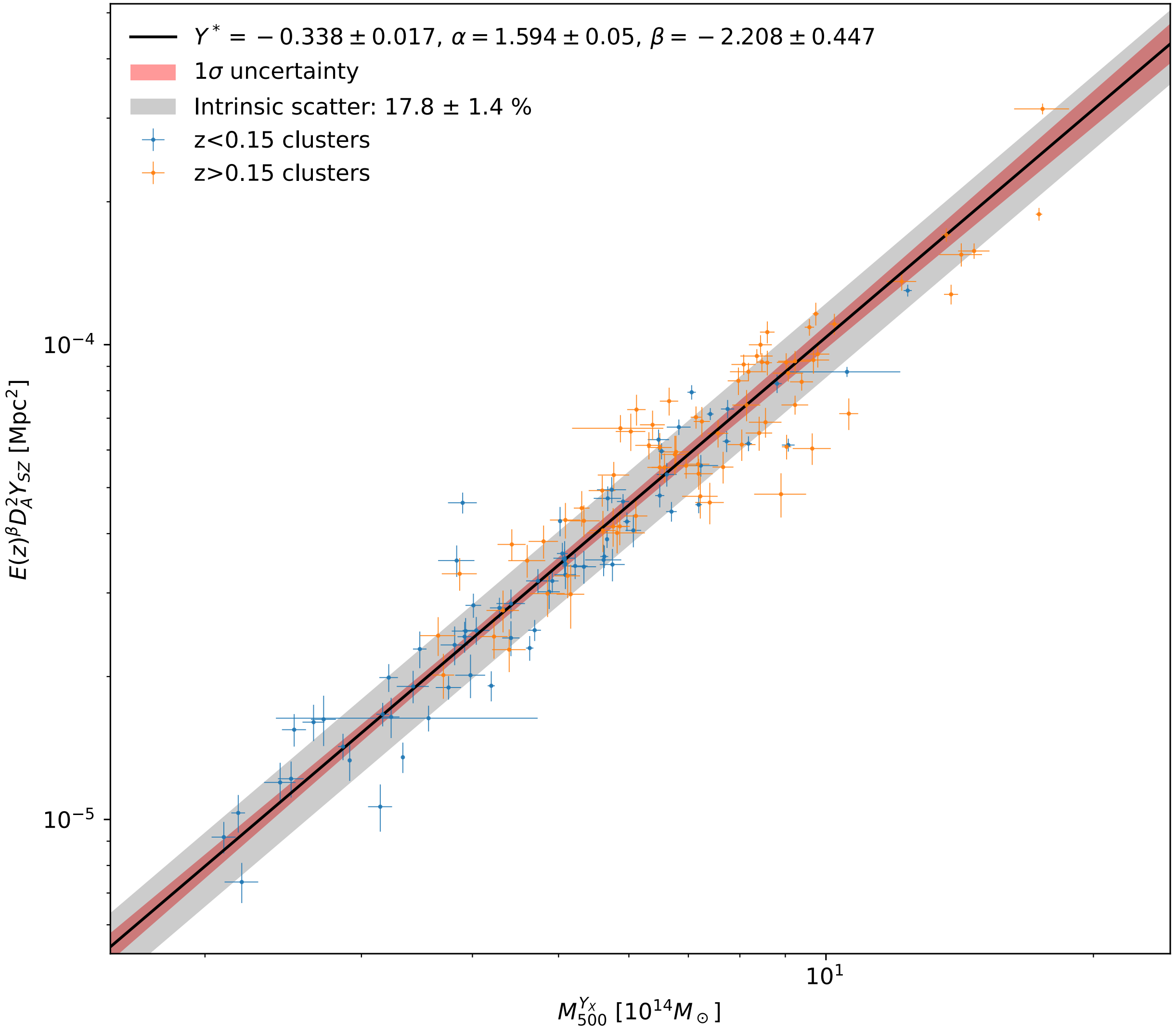

Modify likelihood to allow E(z) exponent to vary:

$$E^c(z)\frac{D_A^2\, Y_{SZ}}{Y_{piv}} = 10^{Y^*}\left(\frac{M_{500}^{Y_X}}{M_{piv}}\right)^{\alpha}$$

Find a **strong preference (3-4 σ)for much higher redshift dependance**

This effect is **not sample-dependent and holds for XMM-Newton calibration sample**

Calibration sample	c
Chandra	-2.22 ± 0.45
XMM-Newton	-1.96 ± 0.47

Including truly high-z clusters would allow for much better understanding of this effect

Bonus: Redshift dependance

Redshift dependance was fixed to self-similar value: can we constrain it from the data ?

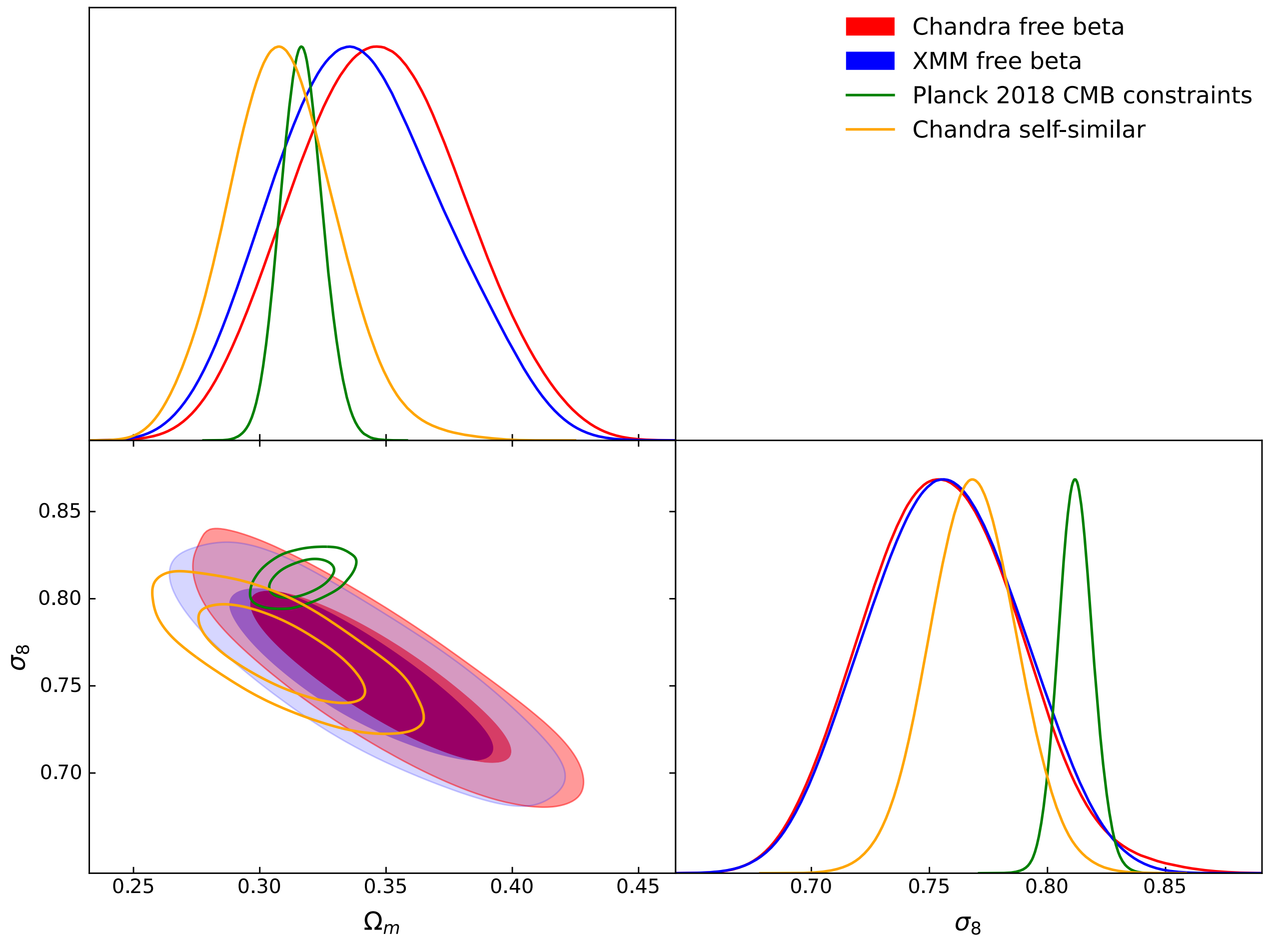

Loss of constraining power, but **preference for higher S_8 values**

Reduction of tension with the CMB constraints

Dealing with projection effects

The functions are made to fit 3D profiles, but observations are 2D projections along the line of sight
During fitting, 3D profiles are first projected then compared to 2D observations

In the case of density/emission integral we can neglect the bin width:

$$EI_i = 2\int_0^{\sqrt{R_{int}^2 - r_i^2}} n_p n_e\left(\sqrt{x^2 + r_i^2}\right) dx \quad \text{where} \quad R_{int} = 50R_{500}$$

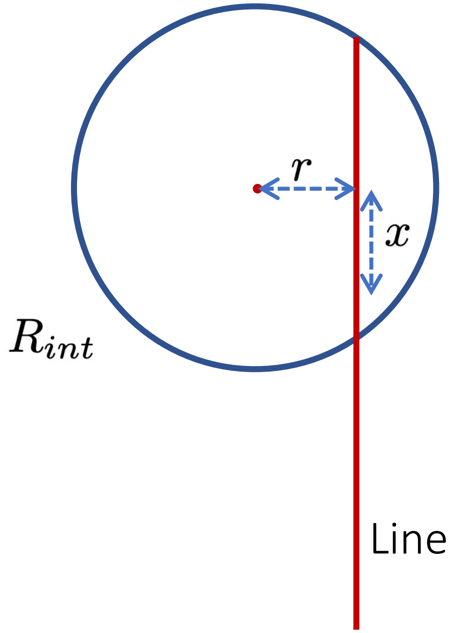

In the case of temperature, we need to weight by density, account for a dependence on temperature (Mazzotta et al. 2004), and take bin width into account:

$$T_i = \frac{\int_{r_i}^{r_{i+1}} \int_1^{\sqrt{(R_{int})^2 - r^2}} r\, w\, T_{\text{fit}}\left(\sqrt{r^2 + x^2}\right) \mathrm{d}x\, \mathrm{d}r}{\int_{r_i}^{r_{i+1}} \int_1^{\sqrt{(R_{int})^2 - r^2}} r\, w\, \mathrm{d}x\, \mathrm{d}r} \text{ where } w = n_p n_e\left(\sqrt{r^2 + x^2}\right) T_{\text{fit}}^{-0.75}\left(\sqrt{r^2 + x^2}\right) \text{ and } R_{int} = R_{200}$$

Masses from X-ray data

With X-ray data, we can compute masses under hydrostatic equilibrium assumption:

$$M_{HE}(< r) = -\frac{r k_B T(r)}{G \mu m_p}\left(\frac{\mathrm{d}\ln\rho(r)}{\mathrm{d}\ln r} + \frac{\mathrm{d}\ln T(r)}{\mathrm{d}\ln r}\right)$$

But clusters’ dynamical states vary widely and the assumption can be quite false

Instead of using the hydrostatic masses, scaling relations are commonly used:

- Calibrate relation between observable/hydrostatic mass for a set of relaxed clusters
- Use the relation to calculate other cluster masses

Appendix

What is the best proxy for mass ?

Kravtsov et al. 2006: comparison of proxies/true mass on simulated Chandra observations of clusters

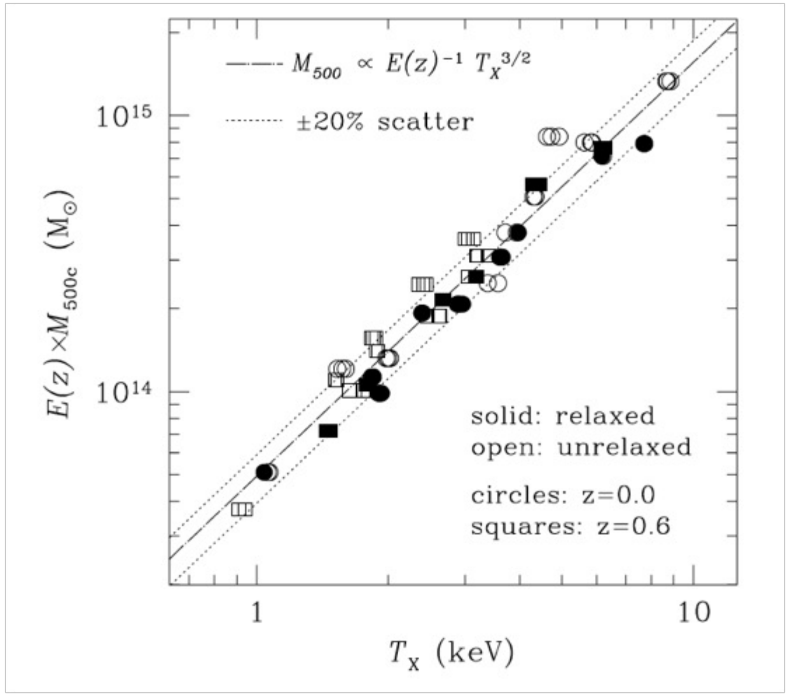

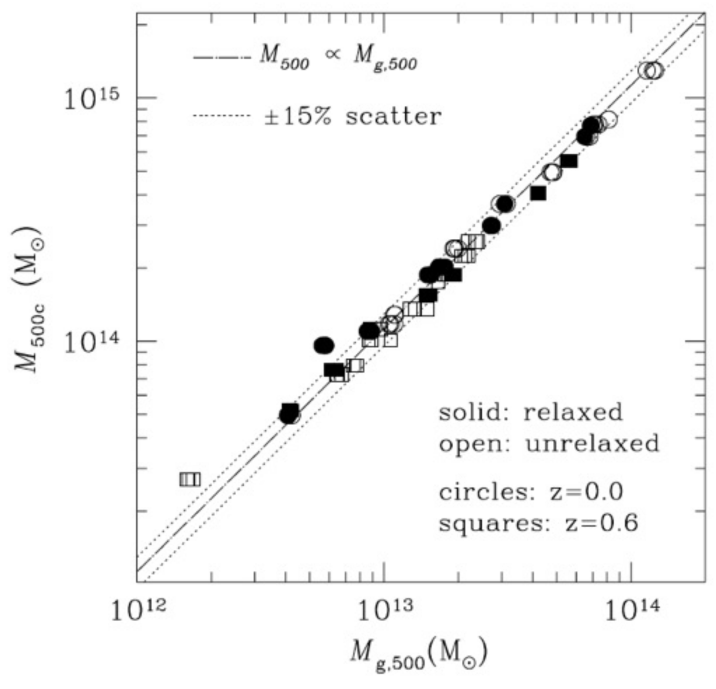

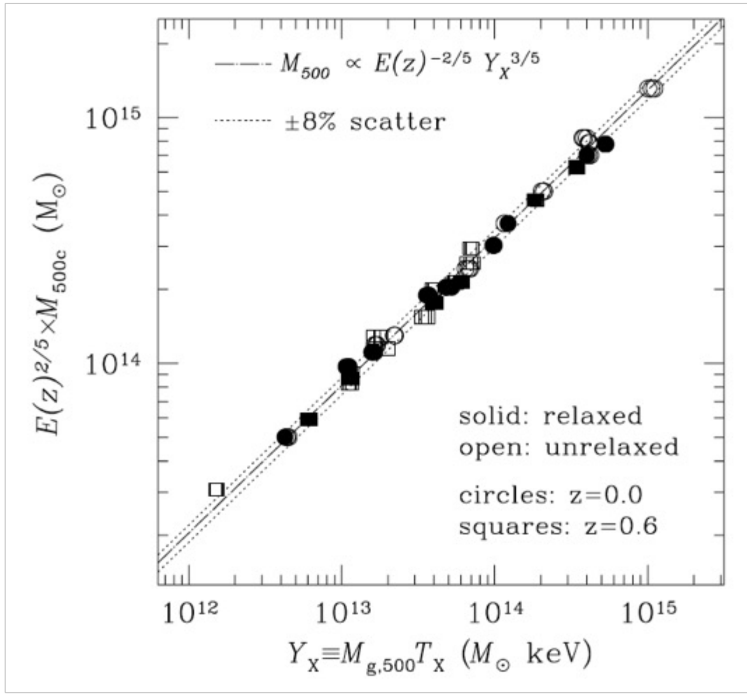

20% scatter due to unrelaxed clusters mostly
Unrelaxed cluster have lower Tx: Kinetic energy not fully converted to thermal during mergers
Slope=self similarity

15% scatter
Slope!=self similarity (0.92+-0.02)
Due to f_gas varying with M&z

8% scatter
No relaxed/unrelaxed distinction
Less sensitive to departure from spherical symmetry
Slope=self similarity

Yx is a robust and self-similar proxy to mass

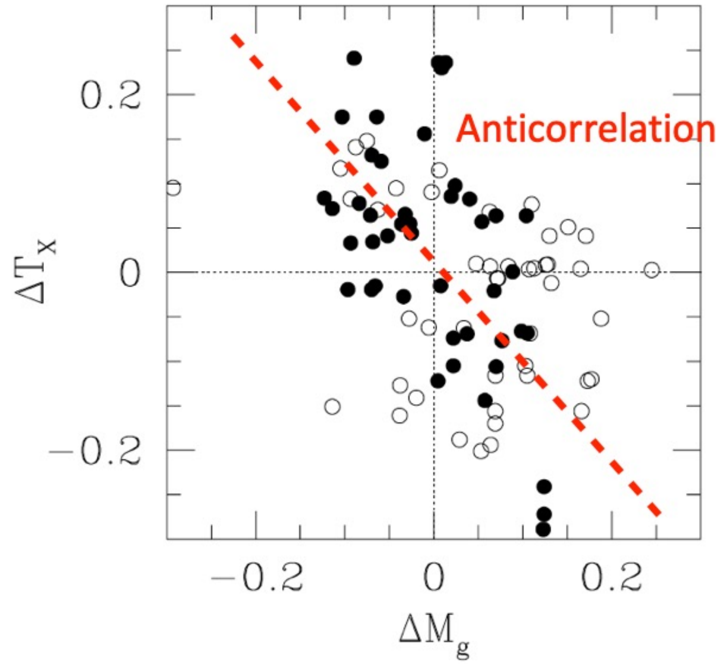

FIG. 5.—Fractional deviations in temperature and gas mass for fixed M_{500} relative to their respective best-fit self-similar relations, $M_{500} \propto T_X^{1.5}$ and $M_{500} \propto M_{g,500}$. The fit includes all systems, at both $z = 0$ (*filled circles*) and $z = 0.6$ (*open circles*). Note that the deviations for gas mass and temperature are generally anti-correlated: clusters with large positive (negative) deviations in $M_{g,500}$ tend to have negative (positive) deviations in T_X. A similar anticorrelation exists in the trend with redshift (compare the distribution of points for $z = 0$ and 0.6). [*See the electronic edition of the Journal for a color version of this figure.*]

Why is Yx a good proxy ?

Less relaxed clusters, over-estimation of Mg (non-uniform density, $\langle n^2 \rangle > \langle n \rangle^2$)

Unrelaxed cluster have lower Tx: kinetic energy not fully converted to thermal during mergers

Analysis of X-ray data

Data processing: from event file to profiles

- Charge-transfer inefficiency, mirror contamination, CCD non-uniformity and time dependence of gain are corrected
- Blank sky and readout artifacts are subtracted
- X-ray point sources and extended substructures are masked
- Surface brightness profile is extracted in the 0.7-2keV band (better signal/noise ratio), in concentric annuli around emission peak
- Spectra are extracted in the 0.6-10keV band, and fitted with single temperature MEKAL model

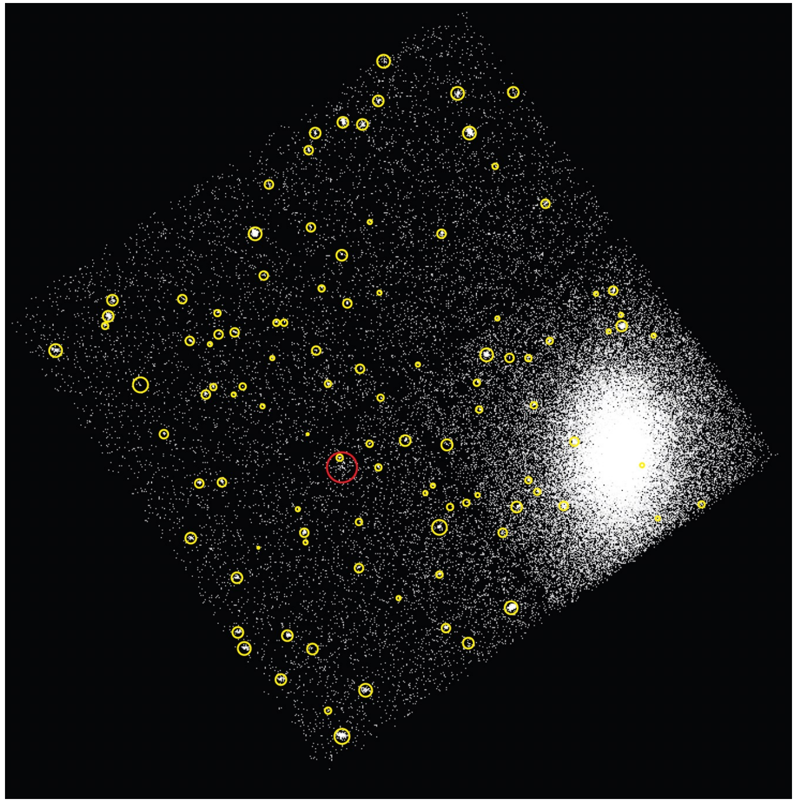

Typical source subtraction, point sources are in yellow and extended source in red

Work done by CfA team (Santos et al. 2021, https://doi.org/10.3847/1538-4357/abf73e)

Analysis of X-ray data

Example of obtained profiles

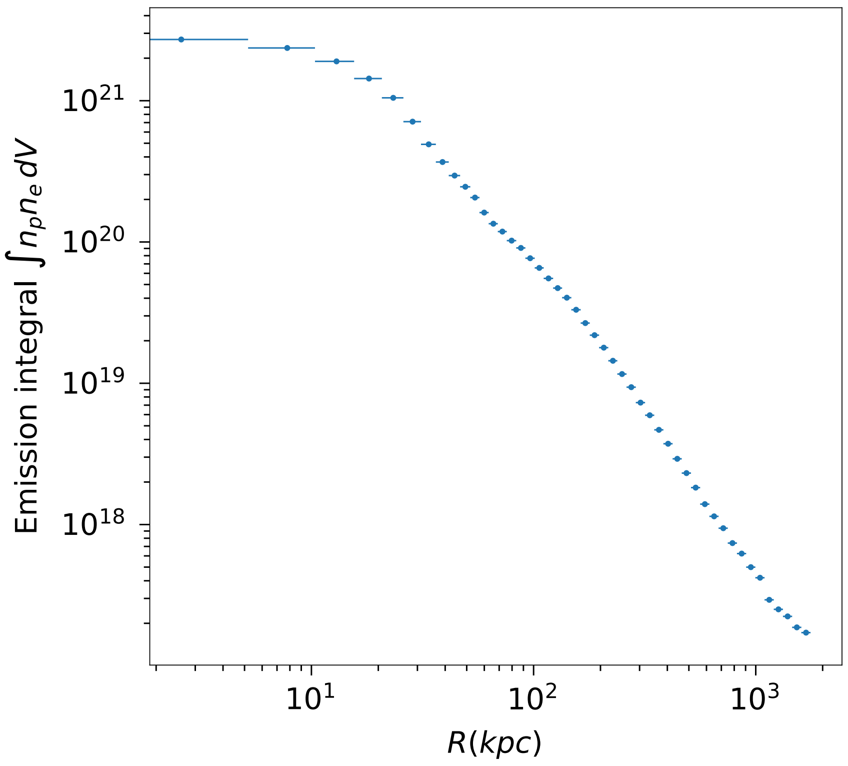

Profile of Abell 2204, z=0.164, high data quality

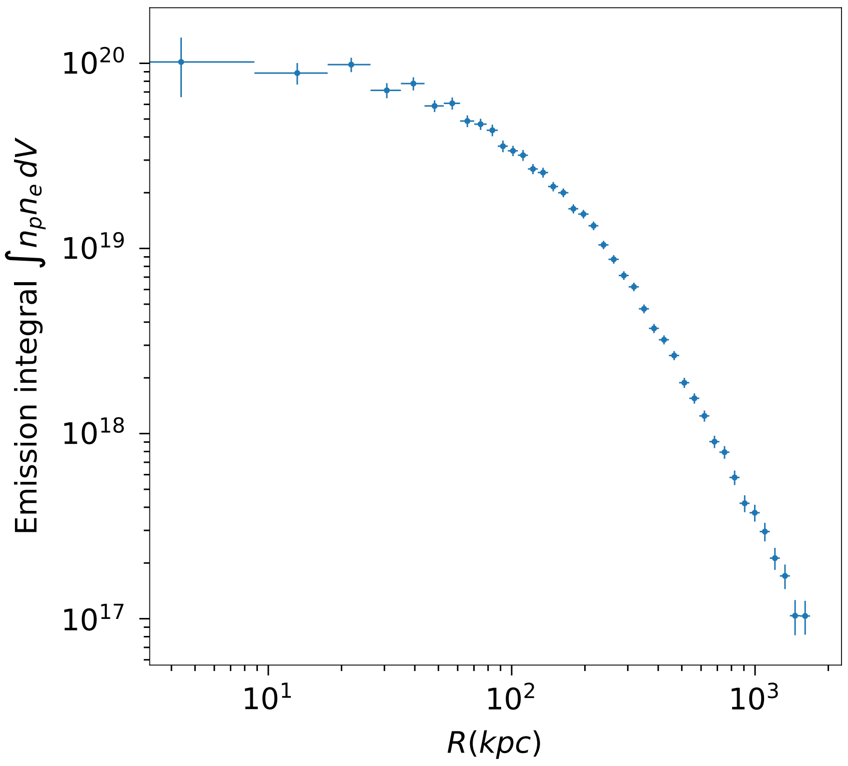

Profile of Abell 2552, z=0.300, low data quality

Work done by CfA team (Santos et al. 2021, https://doi.org/10.3847/1538-4357/abf73e)

Analysis of X-ray data

Calculating masses from X-ray: Yx scaling relation

Use **Vikhlinin et al. 2006 profile for density**:

$$n_p n_e = n_0^2 \frac{(r/r_c)^{-\alpha}}{(1+r^2/r_c^2)^{3\beta-\alpha/2}} \frac{1}{(1+r^\gamma/r_s{}^\gamma)^{\varepsilon/\gamma}} + \frac{n_{02}^2}{(1+r^2/r_{c2}^2)^{3\beta_2}}$$

Project 3D profiles to compare to 2D observations

Calculate masses using Vikhlinin et al. 2009 **Yx-M500 scaling relation**:
Iterative process since Yx is measured within R500:

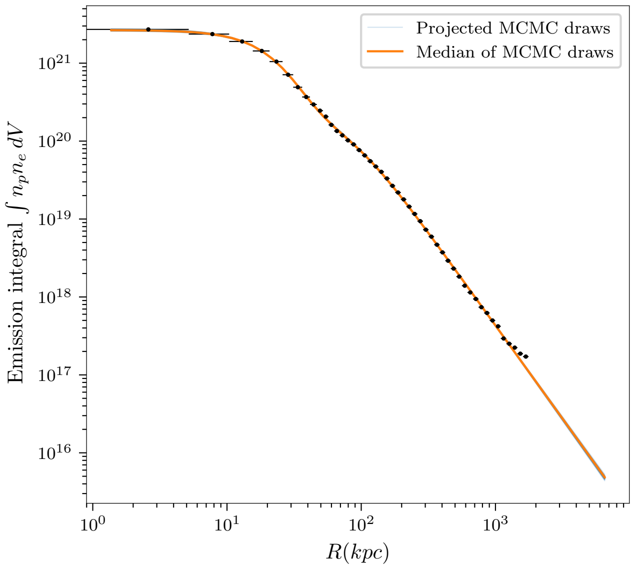

Fitted profile of Abell 2204

Work done by CfA team (Santos et al. 2021, https://doi.org/10.3847/1538-4357/abf73e)

Analysis of X-ray data

Calculating masses from X-ray: Yx scaling relation

Use **Vikhlinin et al. 2006 profile for density**:

$$n_p n_e = n_0^2 \frac{(r/r_c)^{-\alpha}}{(1+r^2/r_c^2)^{3\beta-\alpha/2}} \frac{1}{(1+r^\gamma/r_s{}^\gamma)^{\varepsilon/\gamma}} + \frac{n_{02}^2}{(1+r^2/r_{c2}^2)^{3\beta_2}}$$

Project 3D profiles to compare to 2D observations

Calculate masses using Vikhlinin et al. 2009 **Yx-M500 scaling relation**:
Iterative process since Yx is measured within R500:

1) First R500 value from T-M500 scaling relation (Vikhlinin et al. 2009)

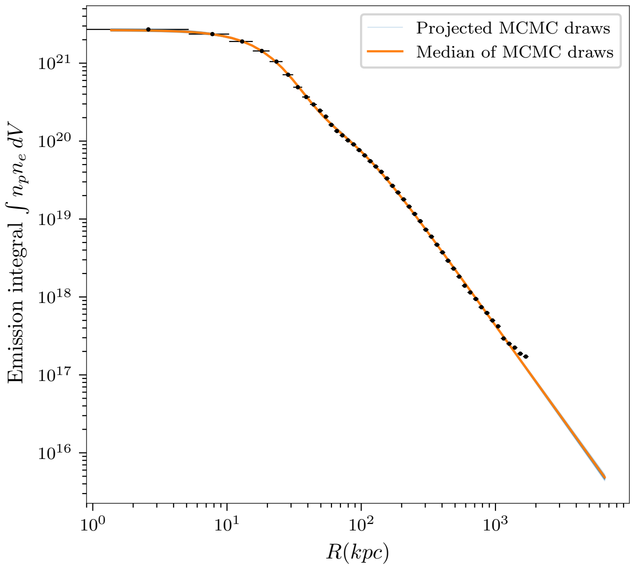

Fitted profile of Abell 2204

Work done by CfA team (Santos et al. 2021, https://doi.org/10.3847/1538-4357/abf73e)

Analysis of X-ray data

Calculating masses from X-ray: Yx scaling relation

Use **Vikhlinin et al. 2006 profile for density**:

$$n_p n_e = n_0^2 \frac{(r/r_c)^{-\alpha}}{(1+r^2/r_c^2)^{3\beta-\alpha/2}} \frac{1}{(1+r^\gamma/r_s{}^\gamma)^{\varepsilon/\gamma}} + \frac{n_{02}^2}{(1+r^2/r_{c2}^2)^{3\beta_2}}$$

Project 3D profiles to compare to 2D observations

Calculate masses using Vikhlinin et al. 2009 **Yx-M500 scaling relation**:
Iterative process since Yx is measured within R500:

1) First R500 value from T-M500 scaling relation (Vikhlinin et al. 2009)

2) Measure core excised Tx in [0.15,1] R500, $Y_X = kT_{exc}\, M_{gas}^{500}$

3) Solve $\frac{4\pi}{3} 500 \rho_{crit}(z) R_{500}^3 = M_{500} = (5.77 \pm 0.20) \cdot 10^{14}\, h^{1/2}\, M_\odot \left(\frac{Y_X(R_{500})}{3 \cdot 10^{14}\, M_\odot \mathrm{keV}} \right)^{0.57\pm0.03} E(z)^{-2/5}$ for R500 (Vikhlinin et al. 2009)

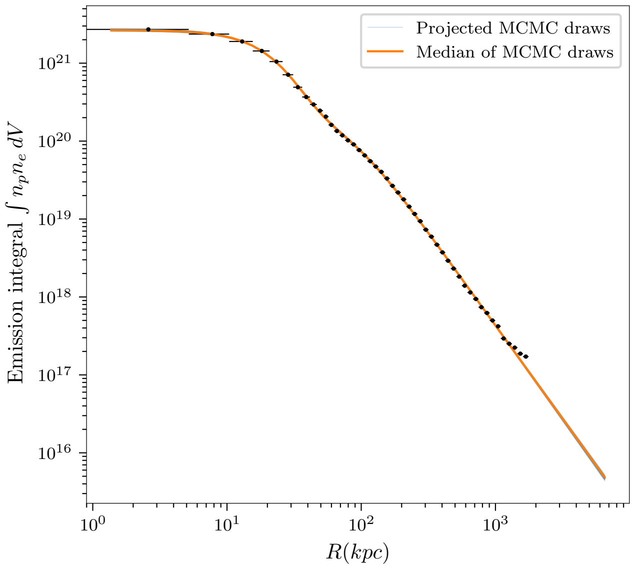

Fitted profile of Abell 2204

Work done by CfA team (Santos et al. 2021, https://doi.org/10.3847/1538-4357/abf73e)

Calculating masses from X-ray: Yx scaling relation

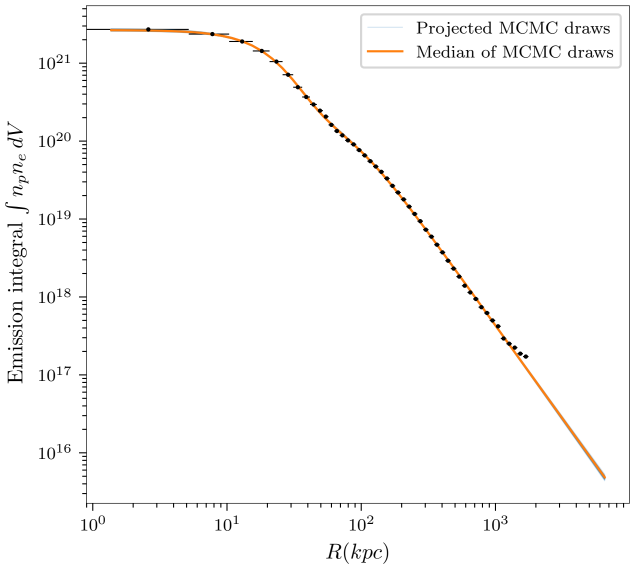

Fitted profile of Abell 2204

Use **Vikhlinin et al. 2006 profile for density**:

$$n_p n_e = n_0^2 \frac{(r/r_c)^{-\alpha}}{(1+r^2/r_c^2)^{3\beta-\alpha/2}} \frac{1}{(1+r^\gamma/r_s{}^\gamma)^{\varepsilon/\gamma}} + \frac{n_{02}^2}{(1+r^2/r_{c2}^2)^{3\beta_2}}$$

Project 3D profiles to compare to 2D observations

Calculate masses using Vikhlinin et al. 2009 **Yx-M500 scaling relation**:
Iterative process since Yx is measured within R500:

1) First R500 value from T-M500 scaling relation (Vikhlinin et al. 2009)

2) Measure core excised Tx in [0.15,1] R500, $Y_X = kT_{exc}\, M_{gas}^{500}$

3) Solve $\frac{4\pi}{3} 500 \rho_{crit}(z) R_{500}^3 = M_{500} = (5.77 \pm 0.20) \cdot 10^{14}\, h^{1/2}\, M_\odot \left(\frac{Y_X(R_{500})}{3 \cdot 10^{14}\, M_\odot \mathrm{keV}} \right)^{0.57 \pm 0.03} E(z)^{-2/5}$ for R500 (Vikhlinin et al. 2009)

4) Iterate 2)&3)

5) $M_{500} = (5.77 \pm 0.20) \cdot 10^{14}\, h^{1/2}\, M_\odot \left(\frac{Y_X(R_{500})}{3 \cdot 10^{14}\, M_\odot \mathrm{keV}} \right)^{0.57 \pm 0.03} E(z)^{-2/5}$

Work done by CfA team (Santos et al. 2021, https://doi.org/10.3847/1538-4357/abf73e)

XMM Newton vs Chandra

Temperature measurements don’t match, leading to different Yx values

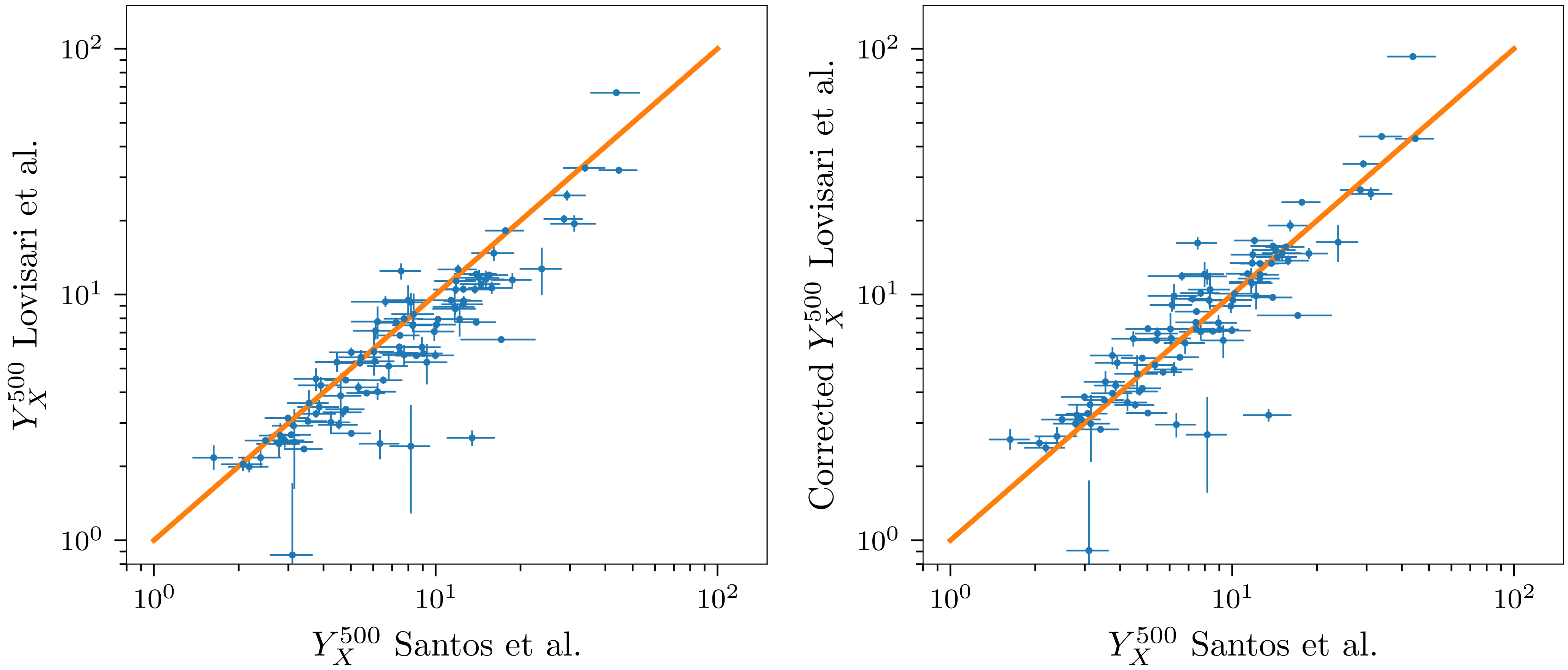

The temperature calibration can be accounted for, but the truth isn’t known

XMM Newton vs Chandra

Because the true temperature isn't known, and Yx-M500 relations relie on HSE hypothesis, the masses inferred from Chandra and XMM differ

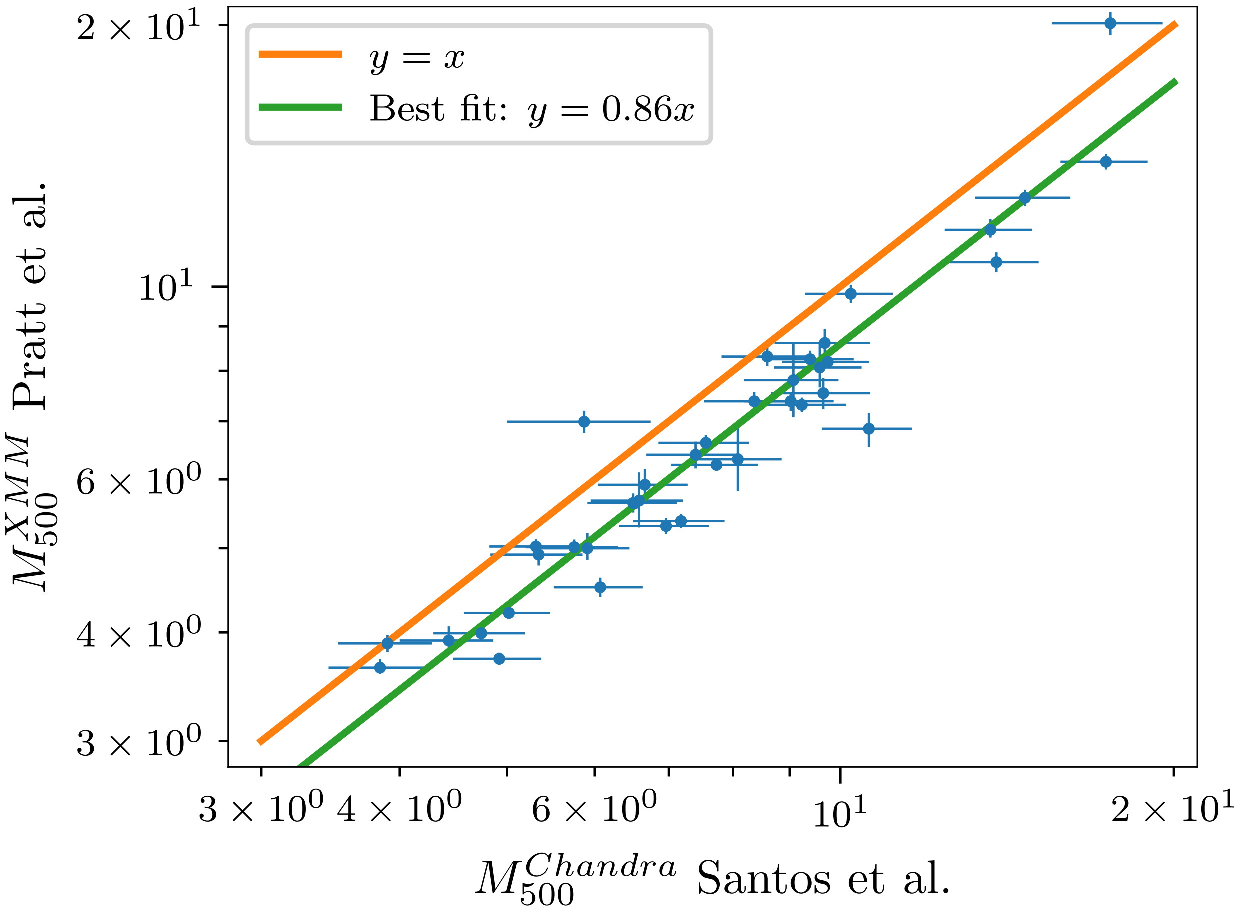

XMM scaling relation (Arnaud et al. 2010):

$$h(z)^{2/5}\, M_{500} = 10^{14.567\pm0.010}\left[\frac{Y_{\mathrm{X}}}{2\times10^{14}\,\mathrm{h}_{70}^{-5/2}\,\mathrm{M}_\odot\,\mathrm{keV}}\right]^{0.561\pm0.018} \mathrm{h}_{70}^{-1}\,\mathrm{M}_\odot$$

Chandra scaling relation (Vikhlinin et al. 2009):

$$M_{500}^{Y_{\mathrm{X}}} = E^{-2/5}(z)A_{\mathrm{YM}}\left[\frac{Y_{\mathrm{X}}}{3\times10^{14}M_\odot\mathrm{keV}}\right]^{B_{\mathrm{YM}}}$$

$$A_{\mathrm{YM}} = (5.77\pm0.20)\times\ 10^{14}h^{1/2}M_\odot$$

$$B_{\mathrm{YM}} = 0.57\pm0.03$$

Schellenberger et al. 2015:

$$M_{500}^{\mathrm{XMM}} = 0.859^{+0.017}_{0.016}\cdot\ M_{500}^{Chandra})^{1.00\,\pm\,0.02}$$

The masses obtained from Yx with XMM are 14% lower on average

Malmquist bias

When studying the relation between signal and another observable for a signal-to-noise limited sample, the intrinsic scatter in the relation will lead to preferential detection of objects biased high w.r.t. the mean in the low signal range

This needs to be accounted for when calibrating a scaling relation, by dividing each Ysz by the mean bias at the corresponding signal to noise ratio

$$Y_{SZ}^{corrected} = Y_{SZ}/b$$

$$\ln b = \frac{\exp\left(-x^2/2\sigma^2\right)}{\sqrt{\pi/2}\,\mathrm{erfc}\left(-x/\sqrt{2}\sigma\right)}\sigma$$

where $x = -\log\left(\frac{(S/N)}{(S/N)_{cut}}\right)$ and $\sigma = \sqrt{\ln[((S/N)+1)/(S/N)]^2 + (\ln 10\,\sigma_{int})^2}$

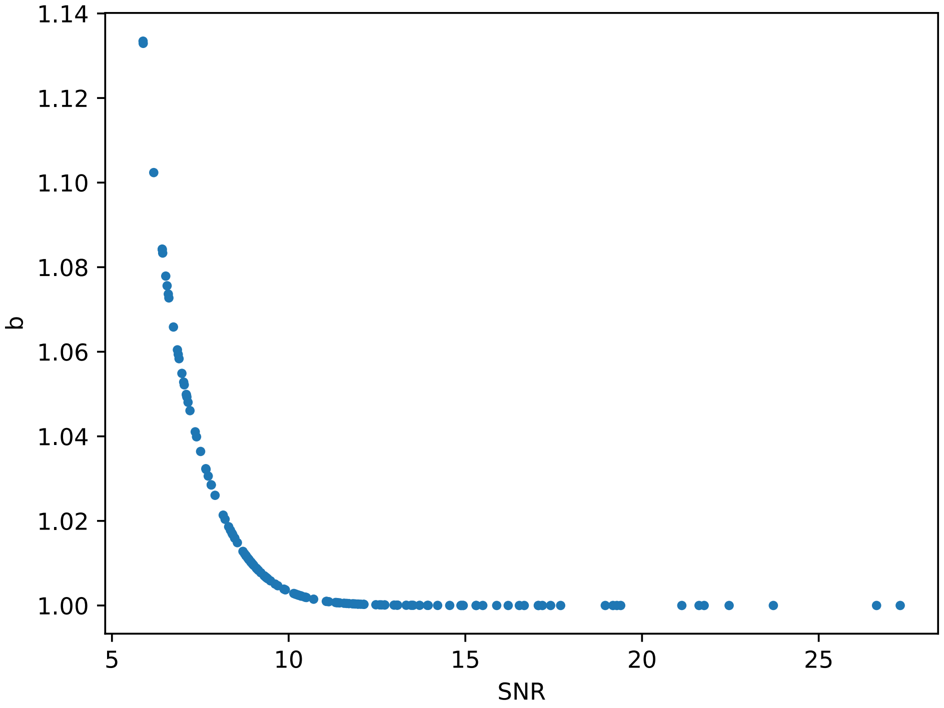

Appendix

What are the effect of changing the scaling relation ?

Lower normalisation: heavier clusters, higher S_8

Change of slope: modifies ratio of high to low mass clusters, moves constraints along σ_8- Ω_m degeneracy